International Journal of Heat and Mass Transfer 155 (2020) 119858

Contents lists available at ScienceDirect

International Journal of Heat and Mass Transfer

journal homepage: www.elsevier.com/locate/hmt

Forced convection heat transfer of Nano-Encapsulated Phase Change Material (NEPCM) suspension in a mini-channel heatsink

C.J. Ho [a,*], Yen-Chung Liu [a], Mohammad Ghalambaz [b,c], Wei-Mon Yan [d,e,*]

[a] Department of Mechanical Engineering, National Cheng-Kung University, Tainan 70101, Taiwan
[b] Metamaterials for Mechanical, Biomechanical and Multiphysical Applications Research Group, Ton Duc Thang University, Ho Chi Minh City, Vietnam
[c] Faculty of Applied Sciences, Ton Duc Thang University, Ho Chi Minh City, Vietnam
[d] Department of Energy and Refrigerating Air-Conditioning Engineering, National Taipei University of Technology, Taipei 10608, Taiwan
[e] Research Center of Energy Conservation for New Generation of Residential, Commercial, and Industrial Sectors, National Taipei University of Technology, Taipei 10608, Taiwan

ARTICLE INFO

Article history:
Received 19 January 2020
Revised 17 April 2020
Accepted 22 April 2020
Available online 3 May 2020

Keywords:
Forced convection
Microchannel heat sink
Water-based suspension
Nano-Encapsulated Phase Change Materials (NEPCMs)

ABSTRACT

In the present experimental study, Nano-Encapsulated Phase Change Material (NEPCM) nanoparticles with particle sizes in the range of 250–350 nm are synthesized. The core of nanoparticles is made of eicosane and can undergo liquid-solid phase change by absorbing/releasing latent heat. The eicosane core of the NEPCM particles is enclosed in a formaldehyde shell, and the particles are suspended in the water as the base fluid. The synthesized NEPCM-water suspension is employed as the working-fluid for heat removal from a microchannel heatsink. The heatsink is made of red-copper, and it consists of eight rectangular microchannels with an aspect ratio of 1.5 and a hydraulic diameter of 1.2 mm. Under the heatsink, a heating plate is embedded, which produces a uniform heat flux. The working-fluid, NEPCM-water, enters the microchannel and absorbs the heat from the microchannel walls in the form of sensible and latent heat. The impact of the nanoparticle's concentration, the heating-power, and the flow rate is investigated on the channel wall temperature, Nusselt number, convection ratio, performance index, and coefficient of performance. The results show that the presence of NECPM-particles improves heat transfer and the index of performance up to 70% and 45%, respectively. The observed enhancement of heat transfer is particularly notable at low Reynolds numbers. However, at the high Reynolds numbers, the presence of NECPM particles may reduce the convection ratio and performance index, which is mainly due to the increase of the viscosity and reduction of the sensible heat of the working-fluid in the presence of NEPCM nanoparticles.

1. Introduction

In recent years, the demand for smaller and lighter electronic components, such as tablet computers, smartphones, has been increased intensively. The miniaturization of electronic components has notably increased the density of heat generation in the constructive tiny chips and electronic circuits. As a result, the conventional passive air cooling systems are not capable of adequate heat removal of such tiny components with a high density of surface heat flux. Hence, active liquid cooling systems are demanded. In this regard, the miniature heat exchangers have received close attention. The millimeter- and micrometer-scale flow channel heatsinks are of important interest due to their very high heat removal capability. Using the liquid as the coolant in miniature heat exchangers not only improves the heat removal capacity of the heat exchanger but also reduces the required pumping power for the circulation of a working liquid in micron-level flow channels. The most direct way to improve the efficiency of small heat exchangers is to use a working liquid with higher heat capacity. The highest magnitude of heat capacity is related to the phase change phenome. So that, in recent years, the suspensions and slurries of Micro-Encapsulated Phase Change Materials (MEPCMs) are introduced. The MEPCM particles are made of a Phase Change Material (PCM) core and a shell, in which the shell acts as a container for liquid/solid PCM core. The PCM core of the particle can phase change by absorbing/releasing heat in the form of latent heat. Hence, a working-fluid containing MEPCM particles can benefit from the latent heat capacity of the phase change core and absorb a notable amount of energy in the form of the latent heat.

* Corresponding authors.
E-mail addresses: cjho@mail.ncku.edu.tw (C.J. Ho), mohammad.ghalambaz@tdtu.edu.vn (M. Ghalambaz), wmyan@ntut.edu.tw (W.-M. Yan).

https://doi.org/10.1016/j.ijheatmasstransfer.2020.119858
0017-9310/

Nomenclature

Latin symbols

A_{ch}	the cross-sectional area of single-channel (m^2)
Ar	*channel aspect ratio defined as Hch/Wch*
COP	*coefficient of performance*
Cp	*specific heat capacity at constant pressure (J/(kg.K))*
df	*uncertainty*
DH	*channel hydraulic diameter (mm)*
f	*friction factor*
FOM	*performance index*
Hc	*the distance between the bottom of the runner and the thermocouple (m)*
$\bar{h}$	*the average convective heat transfer coefficient (W/(m2 .K))*
I	*current (A)*
k	*the thermal conductivity (W/(m . K))*
Lch	*the wet perimeter of the channel, channel length (m)*
N	*the microchannels*
$\overline{Nu}$	*average Nusselt number*
P	*pump power (W)*
p	*pressure (Pa)*
Pe	*Péclet number*
q	*heat removal*
q"	*heat flux (W/m2)*
$\dot{Q}$	*volume flow rate (m3/s)*
Re	*Reynolds number*
Sb	*the subcooling parameter*
*Ste**	*the ratio of the heating-power to the latent heat of the phase change*
T	*temperature (°C)*
TM	*fusion temperature of phase change material (°C)*
um	*average velocity (m/s)*
V	*voltage (V)*
W	*channel width*
x1, x2, xn	*measurements*

Greek symbols

β	*the angle of channel walls (deg)*
Δ	*difference*
ΔH	*the latent heat value of the phase change material*
$\Delta Tref$	*the relative temperature defined as* $q_h/\rho_{bf}C_p\dot{Q}$ *(°C)*
Δx	*measurement error*
ε	*the convection ratio*
θ	*non-dimensional temperature*
μ	*dynamic viscosity (N.s/m2)*
ρ	*density (kg/m3)*
$\omega nepcm$	*the volume fraction of nanoparticles (%)*
ωpcm	*mass fraction of nanoparticles (%)*

subscripts

bf	*base fluid*
ch	*channel*
eff	*calculation using average inlet and outlet hydraulic diameter*
in	*channel inlet*
m	*average*
mtd	*calculation based on the average inlet and outlet temperatures*
nepcm	*nanocapsules phase change material*
out	*channel outlet*
tc	*thermocouple*
w	*the bottom wall of the channel*

The phase change thermal energy storage aspect of phase change materials improved with nanoparticle additives is also another important area, which has been discussed in recent publications for cooling applications [1], solar systems [2,3], and electronic cooling [4].

The microchannel-heatsinks were first proposed by Tuckerman and Pease [5] about 40 years ago. The microchannel-heatsinks show an outstanding heat removal capability. For many years, the working-fluid in microchannels was water, and the geometric appearance of the channels was a rectangular cross-section. By the increase of demand for higher heat removal rate, various methods such as convective boiling [6], using nanofluids [7–10], multipass microchannels [11,12], nanoemulsion [13–16], and a slurry of encapsulated phase change materials [17–19] are introduced. Rao et al. [20] experimentally addressed the heat transfer performance of water-based MEPCM suspensions in a rectangular copper-minichannel with a hydraulic diameter of 2.71 mm. The experiments were performed for the mass concentration of MEPCM particles up to 20% and various mass flow rates. The authors reported that the cooling performance of using MEPCM suspensions depends on the mass flow rate. They found that using a low concentration of MEPCMs particles, i.e., 5%, always improves the heat transfer performance and reduces the wall temperature. However, high concentrations are only effective when the mass flow rates are low. The high concentration MEPCM suspensions lose their thermal advantage at higher mass flow rates. Chow et al. [21] introduced a mathematical model and investigated the impact of using MEPCMs slurries to improve the heat transfer rate in the high heat flux devices, such as Insulated-Gate Bipolar Transistor (IGBT) and Monolithic Microwave Integrated Circuits (MMICs), which are essential in Navy-ships.

Wu et al. [22] dispersed NEPCM particles in poly-α-olefin (PAO) liquid to absorb the thermal energy of the fluid during solid-liquid phase changes. They synthesized two types of slurries, which were bare indium and silica encapsulated indium NEPCMs. The NEPCM suspension could be of practical interest solely for high-temperature applications due to the high fusion temperature of indium particles (150 ~ 180 °C). The heat transfer performance of NEPCM-PAO suspension was examined in a microchannel heat exchanger. The outcomes showed that using 30% of bare indium NEPCM particles resulted in a convective heat transfer coefficient of 47,000 W/m^2 K, which was two-fold of pure PAO.

In another study, Ho et al. [23] utilized a suspension of MEPCMs to improve the heat transfer of a microchannel heatsink. The heatsink was made of copper, which was consisted of 10 minichannels with a rectangular cross-section of 1.5 mm × 1 mm and a length of 50 mm. The flow Reynolds numbers were investigated in the range of 133–1515 with MEPCM mass concentrations of 0 to 10 wt%, while the bottom of the heatsink was subject to a uniform heat flux. When the Reynolds number was small, the presence of MEPCMs was significant and reduced the wall temperature. Moreover, the working-fluid containing MEPCM particles showed a better performance index (cost of performance) compared to the pure coolant. The optimum cooling performance was reported for 2% MEPCM concentration.

Hasan et al. [24] theoretically explored the influence of using MEPCM suspension as a coolant in microchannel heatsinks. These authors investigated the influence of using various core and wall materials as well as different base fluids on the heat transfer enhancement. They addressed the effect of RT44 and n-octadecane as the core-PCMs, and PAO and poly-methylmethacrylate (PMMA) as the shells on heat transfer behavior of the suspension. The base fluids were pure water, oil, or ethylene glycol. The heatsink was subject to a uniform heat flux at the bottom, and the concentration of MEPCM particles was investigated up to 20%. It was found that using MEPCM suspensions could improve the heat transfer by 20.91% for RT44+PMMA in oil, 16.91% for RT44+PMMA in ethylene

glycol, and 12.91% for RT44+PMMA in pure water when the concentration of MEPCMs was 2%.

In another recent work, Ho et al. [25] explored the effect of using MEPCM-suspensions in heatsinks. They reported that increasing MEPCM particle concentration up to 10% improves the heat transfer in the heatsink notably. Recently, by the development of nanotechnology, the Nano-Encapsulated Phase Change Materials (NEPCMs) can be produced [26–28]. Dispersing NEPCM particles in a liquid has the advantage of more-stable suspension, a higher surface of heat transfer between the liquid and nanoparticle, and better thermophysical properties of the suspension. Using nano-size PCM particles greatly reduces the possibility of clogging in the microchannels, increases the heat transfer area of the particles, and the improves the thermophysical properties of the working-fluid.

Zhang et al. [29] theoretically investigated the influence of using NEPCM slurries on the cooling performance of a confined jet array. The working-fluid was PAO, and the NEPCM particles were made of paraffin+polystyrene. The authors reported that micro-convection effect due to the rotation and movement of the microparticles plays an essential role in heat transfer enhancement for MEPCMs, while micro-convection has a minimal impact in nano-scale for NEPCM due to the tiny size of particles. They reported that there exists an optimal volumetric concentration for the best performance of NEPCM particles. Dispersing NEPCM particles first improves thermal performance until it reaches an optimal value. Seyf et al. [30] numerically explored the effect of the presence of NEPCM particles on the thermal performance of NEPCM slurries in microtube heat sinks. These authors also used octadecane for NEPCM and PAO for the working-fluid. The outcomes revealed that using NEPCM notably improved the heat transfer rate, but it also increased the pressure drop. The authors investigated the entropy generation and realized that the presence of NEPCMs reduced the total entropy generation.

In a theoretical study, Petrovic et al. [31] explored the effect of using NEPCM materials and nanofluids as water base working-fluids to enhance the heat transfer in microchannels. Two types of nanoparticles, one made of Cu and the other one made of -Octadecane core (NEPCM), were adopted with various volume fractions up to 5%. They found that using Cu-water nanofluid can provide a better heat transfer rate in the microchannel compared to NECPM nanoparticles. The natural [32–34] and laminar mixed [35] convection heat transfer of NEPCMs suspensions were also investigated in recent theatrical works. The results showed that the presence of NEPCMs particles improved the natural or mixed convection heat transfer. The enhancement was a function of fusion temperature and there was an optimum fusion temperature for maximum heat transfer enhancement.

The literature review shows that the subject of using suspension or slurries of MEPCMs has received a considerable amount of attention for the thermal enhancement of heatsinks in recent years. However, the synthesize of NEPCMs particles has been developed very recently, and thus, there are only very few published works on the thermal benefit of NEPCM-suspensions. Most of the previous works were theoretical works [29–31], and the experimental works were limited to PAO base fluids [22] with indium PCM particles. The indium particles were only applicable for high-temperature ranges above 150 °C. Such a temperature range is not practical for the cooling of electronic components. Hence, the present study aims to experimentally address the thermal performance of NEPCMs in microchannels for electronic cooling applications of micro heatsinks.

2. Experimental method

2.1. Experimental setup

The present experiment aims to study the impact of using NEPCMs on the thermal performance of water in a micro heatsink. Hence, a suspension of NEPCM is synthesized with various mass fractions and used as a working-fluid, which circulates in a closed-loop system as the cooling medium. The working-fluid absorbs a significant amount of heat by passing through a micro heatsink and then cools down in a heat exchanger.

The experimental setup consists of a micro heatsink test-module, measurement system, heat exchangers, a centrifugal pump, and the working-fluid. A schematic view of the experimental setup is depicted in Fig. 1. The centrifugal pump is used to drive the working-fluid and circulate it in the experimental loop. When the working-fluid leaves the pump, its temperature is controlled by a heat exchanger, which is placed in a constant temperature tank. Then, the working-fluid reaches the inlet of the test module and passes through the microchannels of the heatsink.

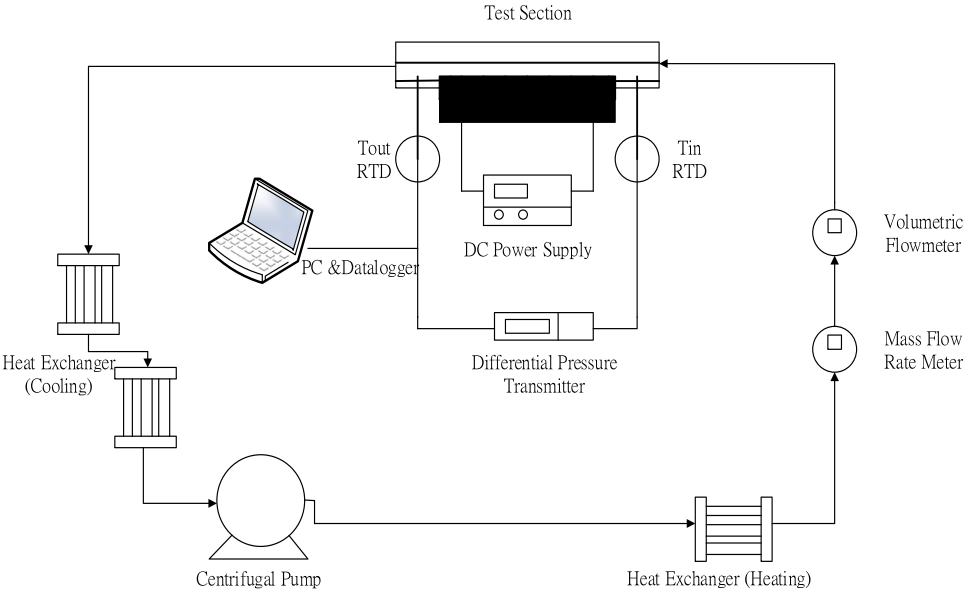

Fig. 1. The schematic view of the experimental setup.

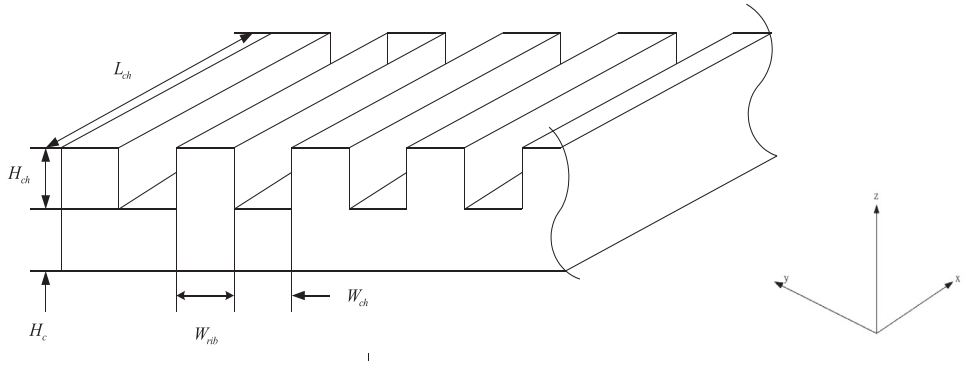

Fig. 2. .The schematic figure of the channels.

In the test module, the fluid absorbs the heat from the heatsink until it reaches the outlet. After the outlet, there is a series of heat exchangers, which are placed in constant bath cool-tanks. These heat exchangers ensure that all of the phase-change material of NEPCM-suspension are entirely solidify. To ensure all of the NEPCMs are well solidify, the temperatures of these cooling bathes are well below the fusion temperature of NEPCMs. Hence, as mentioned, a heating heat exchanger was placed before the inlet of the test module to raise the working-fluid's temperature to the experiment temperature.

A mass flow meter and a volume flow meter are placed after the heating heat exchanger and before the inlet of the test module to measure the flow rate. Finally, to control the experimental conditions, the entire experimental loop is covered with cotton as the thermal insulation to reduce its environmental heat loss. The pressure-drop through the heatsink test-module is measured by using a differential pressure sensor, placed at the inlet and outlet of the test-module. The inlet and outlet temperatures of the test-module are measured by using thermocouples.

The micro heatsink is made of oxygen-free copper (the thermal conductivity coefficient is 401 W/m.K), and it consists of 8 rectangular cross-section parallel microchannels. Here, β is the angle of the microchannel walls, which is zero in the present study. The wall thickness of the channels is 0.25 mm. The cutting electric discharge machine (Wire EDM) initially carved the channels in the heatsink with a width of 0.8 mm and a height of 1.3 mm. Then, a CNC milling machine is used to precisely cut the channels with a width of 1.0 mm and a height of 1.5 mm and with a tolerance of 0.1 mm. The hydraulic diameter of each channel is 1.2 mm, with an aspect ratio of 1.5. The schematic figure of the channels is depicted in Fig. 2. Here β° denotes the angle of the channel's walls, which is zero in the current research as the channel-walls are parallel. The geometrical details of the heatsink are summarized in Table 1. Here, N denotes the number of channels, and A_r indicates the channel's aspect ratio (height/width).

As mentioned before, Ho et al. [10] investigated the heat transfer of Alumina nanofluids in microchannel heatsinks. They reported that using copper as a holder of the heatsink increases the heat loss as it is highly thermal-conductive. Hence, the copper cannot be used as a fixture to hold the heatsink in place. One of the good options to fix the heatsink was acrylic, which was used in some of the literature studies, but the heat-resistant temperature of acrylic is as low as 80 ºC. When the input power of this experiment is 30 W, the temperature can be reached to 90 ºC. Therefore, the acrylic is not suitable for the present experiment. Hence, Teflon was adopted as the fixture to hold the heatsink. The heat-resistant temperature of Teflon is up to 150 ºC, which is adequate for the present experiment. A layer of acrylic is utilized as extra insulation. The acrylic is selected for the top led of the channel. The selection of the acrylic for the top cover is possible since the heat transfer between the working-fluid and the channel walls reduces the temperature of top channel walls much below 80 ºC. Using acrylic as top cover facilities the direct observation of NEPCM flow in the channel and also provides good insulation to prevent heat loss.

Table 1
The geometrical details of the heatsink and channels.

Property	W_{ch}	H_{ch}	W_{rib}	D_h	L_{ch}	H_c	A_r	N
Value (mm)	1.0	1.5	1.5	1.2	50	5	1.5	8

In the present study, two heating plates are used at the bottom of the heatsink. The heating plates are divided into the main heating plate and the compensation heating plate. The main heating plate provides the heat flux at the bottom of the heatsink to simulate the uniform heat flux thermal boundary condition. The second heating plate, which is attached to the back of the main heating plate, compensates for the heat losses. The purpose is to reduce the conduction heat loss caused by the temperature difference and increase the insulation effect. In such a way, it can be ensured that the flow channel completely absorbs the produced heat flux of the main heating plate. The dimensions of the heating plates are 20 mm $\times$ 50 mm, with a thickness of 6 mm.

In this study, two T-type thermocouples are placed at two ends of the mini-channels to measure the temperatures at these regions. In addition, the bottom of a channel of the heatsink is processed by a CNC milling machine along the flow direction to facilitate the placement of thermocouples. A total of 7 thermocouples are confined at a distance of 5 mm under the base surface along the centerline of the mini-channel heat sink. The thermocouples are used to measure the temperature distribution of the channel. By using the measured temperatures and invoking the one-dimensional heat conduction approach, the temperature of the bottom wall of the channel can be estimated along the flow direction. The geometric configuration of the thermocouples is illustrated in Fig. 3. Moreover, a thermocouple is placed at the inlet, and another one is placed at the outlet to measure the inlet and outlet temperatures of the working-fluid. Hence, the net amount of the absorbed heat by the working-fluid can be calculated by using the inlet and outlet temperatures of the working-fluid.

It should be noted that the conduction heat transfer is the main mechanism of heat transfer between the main heating plate and the heatsink. Hence, some thermal paste is added between the heatsink and the main heating plate, and the heating plate is tightly and uniformly attached to the heatsink by a uniform pressure of an external clamp. Ten extra stainless steel screws are used to lock the Teflon clamp to the microchannel tightly.

Moreover, waterproof tape and high-temperature gasket adhesive are used at the joints to ensure that the entire flow channel

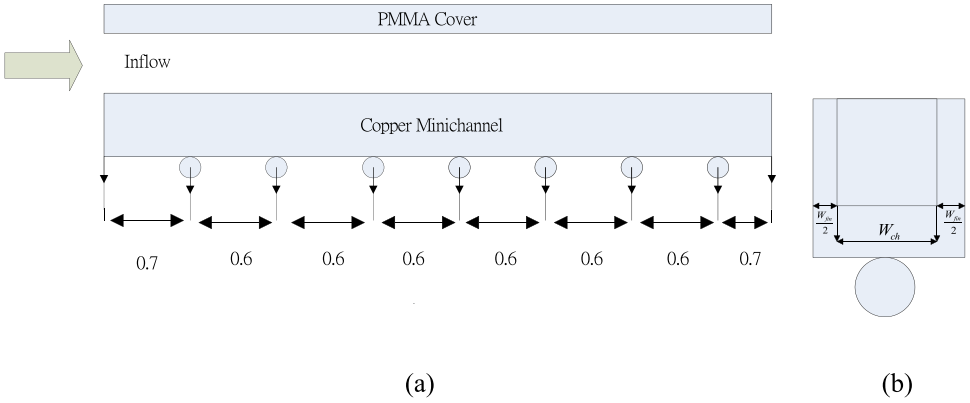

Fig. 3. The thermocouple configuration at the bottom of the heatsink, (a) the location of thermocouples along the length of the channels, (b) the location of the thermocouples below a channel.

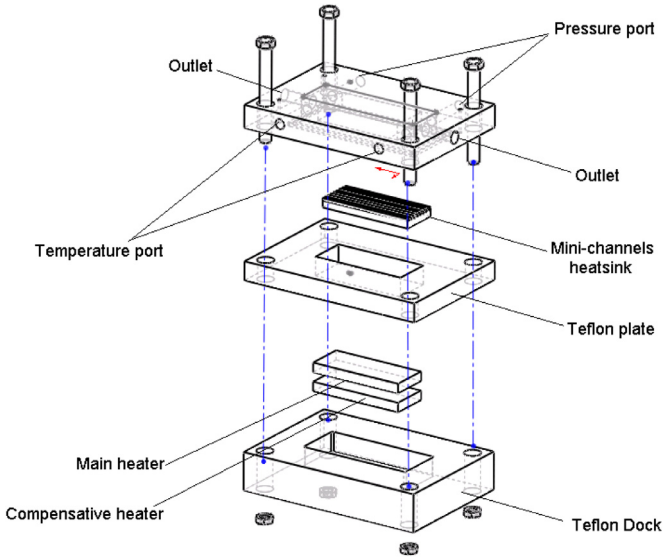

Fig. 4. The schematic diagram of the test module.

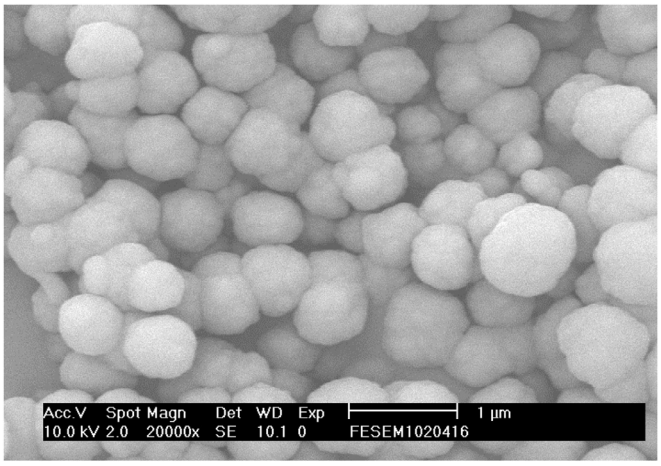

Fig. 5. The Scanning Electron Microscopy (SEM) image of NEPCM powder.

will not cause fluid leakage under high pressure and high temperatures. The overall configuration of the test module is depicted in Fig. 4. A DC power supply is employed to drive the heating plates.

2.2. Working-fluid preparation

The working-fluids in the present experiment are the pure fluid and the water NEPCM-suspension. The NEPCM particles are synthesized as a part of the working-fluid preparation. The interfacial condensation polymerization method used in the preparation of NEPCM particles following the study of Cheng [36]. The eicosane and formaldehyde are adopted as the core and the shell materials, respectively. The ultrasound method is adopted to prepare the emulsion. The ratio of the shell material is adjusted following Cheng [36] to reduce the particle size further to reach the nanoscale. The preparation of the NEPCM-suspension follows three steps of emulsion preparation, shell prepolymer preparation, and capsule coating process. The details of the preparation process can be found in Cheng [36].

The NEPCM suspensions are synthesized using a dried powder of nanocapsules. The NEPCM-suspensions are prepared by mixing a measured value of the dry powder of the capsules in water and stirring with a magnetic stirrer for 30 min. Following [37], the ratio of the core material to the shell material is 1:1. The experimental study of MEPCMs shows that employing a high proportion of the shell material improves the rigidity of the microcapsules [37]. Although the shell material of this experiment is different from that of Su et al. [37], the same trend is still valid. It is found through measurements that if the amplitude of the ultrasonic is too large and the time is too long, the shell of the nanocapsules may be damaged. In such a case, the PCM may leak out, and the prepared suspension becomes a phase-change emulsion suspension. Therefore, by try and error and after several attempts, the ultrasonic time is controlled to 30 min for the best performance and avoiding the shell damage of NEPCM particles. Using this process, various concentrations of NEPCM-suspensions are obtained.

The size of NEPCM particles is measured using Scanning Electron Microscopy (SEM) images. Here, the nanocapsules are non-metallic powders, so they need to be fixed on the coin with carbon tape, and then the surface shall be plated with gold or platinum to increase its conductivity. In the process of sample preparation, the amount and thickness of the dry powder, the amount and thickness of the powder sample have a significant effect on the observation. Besides, if there is any residual moisture, it will considerably affect the observations. The time and uniformity of the gold plating mainly affect the conductivity of the samples and, consequently, the resolution of the measurement. The SEM image of a sample of NEPCMs is depicted in Fig. 5. As shown in Fig. 5, after applying the carbon tape and fixing the dry powder, it feels that there is an obvious stacked. In this case, the size of the capsules is about 500 nm, which is estimated to be larger than the actual capsule

Table 2
The thermal properties of NEPCM-suspensions.

ω_{nepcm} (%)	ω_{pcm} (%)	ρ (kg/m^3)	c_p (J/kg.K)	k (W/m.K)	$\mu \times 10^3$ (N.s/m^2)
0	0.0	994	4180	0.602	0.8
1	0.63	996	4140	0.6	0.97
2	1.8	999	4080	0.59	1.16
5	3.8	1020	3960	0.57	1.25

sizes due to the effect of stacking. Hence, the TEM (Transmission Electron Microscopy) and DLS (Dynamic Light Scattering) measurements are also performed. The results show that the NEPCM particles are almost within a uniform size of 250–350 nm.

In addition to the particle size, the thermophysical properties of the working-fluid, including the specific heat, density, thermal conductivity, and dynamic viscosity, are essential properties that are used in the post-processing analyses of the present study. The thermophysical properties of the NEPCM-suspension are measured and reported in Table 2. The viscosity was measured by using Brookfield DV-II + Pro-Programmable Viscometer, which is a cone and disk type viscometer. The thermal conductivity was measured using Decagon KD2 Pro. This instrument uses the principle of the transient hot-wire method to measure the thermal conductivity of the sample. For the density measurement, a digital liquid density meter (KEM DA-505) and a suspension type densitometer are used.

The results of Table 2 show that there is no significant difference between the thermophysical properties of NEPCM-suspensions compared with the physical properties of water, due to the small concentration of the nano-capsules in the suspension. Since the density of nanocapsules is higher than that of pure water, the higher the concentration of the nano-capsules, the higher the density of the suspension. The presence of NEPCM particles reduces and increases the thermal conductivity and dynamic viscosity of the NEPCM-suspension, respectively. However, the variation of the thermal conductivity of the suspension is minimal, and hence, the thermal conductivity of the suspension can be considered constant.

2.3. Experimental preparation and experimental process

To ensure that each experiment is performed under the same conditions, the following steps are performed before commencing the experiment. First, the working-fluid is drained from all the pipes in the experimental loop, and then the pure water is introduced into the loop and later discharged. After that, the pure water introduced in the test loop and the heaters are turned on until the temperature of the inlet section reaches to the experiment's temperature. For the case of experimenting with pure water, the experiment can be followed after this step. However, in the case of NEPCM working-fluid, the pure water drained, and the NECPM suspension introduced into the cycle. This procedure ensures there is no blockage or leakage during the experiment.

After completing the experimental preparations, the following procedure was followed during the experiments. The gas in the pipelines exhausted, and the pipelines are completely filled with the working-fluid. Then, the differential pressure gage was reset to zero. The flow rate and the temperature of the heat exchangers are set, and the pump is turned on. Then, the inlet temperature of the test module is monitored to reach the experiment's temperature. The heating plates in the test-module are turned on and adjusted to the experimental power setting. The temperature and pressure changes with the data acquisition device are monitored. After the temperature and the pressure reached a steady-state (about 15–20 min), the experimental data are recorded. After each experiment, the experimental loop is cleaned by using pure hot water.

3. Analysis of experimental data

3.1. The utilized relations

In the present study, the Reynolds number is introduced based on the hydraulic diameter of the channel as:

$$\mathrm{Re} = \frac{\rho u_m D_H}{\mu} \tag{1}$$

where u_m is the average velocity $u_m = \dot{Q}/NA_{ch}$. Here, D_H is the hydraulic diameter, defined as $D_H = 4 \times A_{ch}/L_{ch}$, in which A_{ch} and L_{ch} are the cross-sectional area of the channel and the wet perimeter of the channel, respectively. $\dot{Q}$is the volumetric flow rate, N is the number of the microchannels in the micro heatsink, and there are eight microchannels in the current heatsink. The Reynolds number in the present study is in the range of 112~940.

The temperature at the bottom wall of the microchannel is estimated by using the one-dimensional heat conduction equation from the position where the thermocouple is confined in the bottom of the microchannel. The bottom wall temperature of the microchannel is computed as:

$$T_w = T_{tc} - \frac{q''_{eff} H_c}{k_{ch}} \tag{2}$$

where $q''_{eff}$is the heat flux at the bottom of the heatsink the microchannel. The heat flux, q''_{eff}, is estimated as the heating plate heat flux divided by the surface area of the heatsink. Here, H_c is the distance between the thermocouple and the bottom of the microchannel. The non-dimensional temperature (θ_w) can be introduced as

$$\theta_w = (T_w - T_{in})/\Delta T_{ref} \tag{3}$$

where ΔT_{ref} is the relative temperature and is defined as follows.

$$\Delta T_{ref} = \frac{q_h}{\rho_{bf} C_p \dot{Q}} \tag{4}$$

Pump power, which is required to send the working-fluid into the heatsink, is evaluated as

$$P = \Delta p \dot{Q} \tag{5}$$

which is the product of the measured pressure difference across the heatsink (Δp) and the volume flow rate. The friction factor is the ratio of viscous force to hydrodynamic pressure and is defined as follow:

$$f = \frac{1}{2}\frac{D_H}{L_{ch}}\frac{\Delta p}{\rho u_m^2} \tag{6}$$

where L_{ch} is the length of the microchannel, and $\Delta p$is the measured pressure difference across the heatsink. The Nusselt number is introduced using the wall temperature for the inlet and outlet temperature as:

$$\overline{Nu}_{mtd} = \frac{\overline{h}_{mtd} D_H}{k} \tag{7}$$

where the average value of the convection heat transfer coefficient ($\overline{h}_{mtd}$) and is calculated as$\overline{h}_{mtd} = q''_{eff}/(\overline{T}w - (T_{in} + T_{out})/2)$. Here, T_{out} is the outlet temperature. In the heatsink, the microchannels

Table 3
The uncertainties of the present experimental study.

Item	Symbol	Range	Error
Input			
Voltage (Volt)	V	16~26.2	± 0.05 Volt
Current (Ampere)	I	0.65~1.15	± 0.005 Ampere
Length of microchannel (mm)	L_{ch}	50 mm	± 0.2 mm
Hydraulic diameter(mm)	D_H	1.2 mm	± 0.1 mm
Mass fraction (%)	ω_{pcm}	0.63~3.8	± 0.0001%
Measured			
Volume flow rate (m^3/s)	$\dot{Q}$	8.33E-07~0.000007	± 0.1~1.1 (%)
Pressure drop (Pa)	ΔT	200~6900	± 10 Pa
Temperature (K)	T_{tc}	38.5~86.3	± 0.3 K
A difference between inlet and outlet temperatures	ΔT	0.35~8.3	± 0.3 K
Result			
Avg. heat transfer coefficient ($W/(m^2K)$)	$\bar{h}_{mtd}$	782~ 4529	± 6.2~15(%)
Pumping power	P	0.80041E-05~0.0047	± 1.2~15.8(%)
Avg. Nusselt number	$\overline{Nu}_{mtd}$	2.45~9.02	± 6.8~15.9 (%)
Convection ratio	$\varepsilon_{\bar{h}_{mtd}}$	0.7~1.71	± 8.2~25.6(%)
COP	COP	2224~589,094	± 5.5~22.5(%)
FOM	FOM	0.61~1.47	± 5.6~23.8(%)

remove the heat from the main heating plate by conduction mechanism, and hence, the actual heat taken away is divided by the total number of microchannels. The convection ratio ($\varepsilon_{\bar{h}_{mtd}}$) is evaluated as:

$$\varepsilon_{\bar{h}_{mtd}} = \frac{\bar{h}_{mtd,nepcm}}{\bar{h}_{mtd,bf}} \tag{8}$$

The convection ratio represents the ratio of the convective heat transfer coefficient of the working-fluid after the addition of the capsule ($\bar{h}_{mtd,nepcm}$) to that of the base fluid ($\bar{h}_{mtd,bf}$). The convection ratio higher than the unit shows the improved heat transfer by using NEPCM particles. The Coefficient of Performance (COP) is counted as the ratio of the actual heat removal (q_{eff}) to the consumed pumping power (P) as:

$$COP = \frac{q_{eff}}{P} \tag{9}$$

The performance index (FOM, Figure of Merit) is computed as:

$$FOM_{mtd} = \frac{\varepsilon_{\bar{h}_{mtd}}}{(P_{nepcm}/P_{bf})^{\frac{1}{3}}} \tag{10}$$

where FOM_{mtd} is defined as the ratio of the convection ratio ($\varepsilon_{\bar{h}_{mtd}}$) to the pump power ratio performance (P_{nepcm}/P_{bf}). The other cooling parameters are introduced follows:

$$Sb_{in} = \frac{T_M - T_{in}}{\Delta T_{ref}}, Ste* = \frac{c_p \Delta T_f}{\Delta H}, Pe = \frac{\rho c_p u_m D_H}{k} \tag{11}$$

where Sb_{in} is the subcooling parameter, which is defined as the difference between the inlet temperature (T_{in}) and the melting temperature of the phase change material (T_M) divided by the relative temperature (ΔT_{ref}). The subcooling parameter represents the dimensionless value denoting the subcooling degree of the working-fluid before entering the test-module. The Stephan number (Ste^*) is the ratio between the heating-power and the latent heat value of the phase change. In this work, the larger the Stephen number, the higher the heating-power. Here, ΔH is the latent heat value of the phase change material. The phase change material used in this study is eicosane, and the latent heat value is 247.3 J/g. The Peclet number (Pe) is defined as the ratio of momentum diffusion to temperature diffusion and is the product of Reynolds number and Prandtl number.

3.2. Experimental uncertainties

In the current experimental work, the measurement devices and sensors are calibrated before the experiments. Here, the error sources are mainly system errors (bias errors) and random errors (random errors or precision errors). Data processing is performed by taking into account the measurement errors using the following relation:

$$df(x_1, x_2, \cdots x_n) = \sqrt{(\Delta x_1 \frac{\partial f}{\partial x_1})^2 + (\Delta x_2 \frac{\partial f}{\partial x_2})^2 + \cdots\cdots + (\Delta x_n \frac{\partial f}{\partial x_n})^2} \tag{12}$$

where df is the uncertainty of a property to be computed and Δx denotes the error of measurement.

Table 3 shows the error after processing the experimental measurement data. Here, the temperature, voltage, current, pressure drop, volume flow rate, and mass flow rate are the physical parameters, while the length of the flow channel, the width of the flow channel, and the hydraulic diameter are the geometric parameters. The error between voltage and current is one-half of the minimum scale. The volume flow rate part is considered as the error of the volume flow rate because the manual of the flowmeter only provides the error of the average flow rate. Data processed parameters, including inlet and outlet temperature, average wall temperature, convection ratio, Nusselt number, pump power, Reynolds number, and friction factor, are presented with relative errors.

From the analysis of the error, it can be found that the temperature difference between the inlet and outlet temperature is too low when the heating-power is low, or the flow rate is too high. Since the actual amount of the heat transfer is estimated by the temperature difference between the inlet and outlet, this error increases by the increase of the flow rate, and consequently, the error of the wall temperature computations will grow.

Considering the differential pressure, its resolution is only up to ± 10 Pa, so the differential pressure error is larger at low flow rates. The geometric errors are about 0.2 ~ 0.3 mm, which are due to the error of the machine factory and the error of human operation.

4. Results and discussion

The impact of using NEPCM suspension on the microchannel wall temperature, outlet temperature, and the pressure difference is investigated experimentally for various heating-power and flow rates. The results are reported for various mass fractions of PCMs, 0% (pure water), 0.63%, 1.8%, and 3.8%.

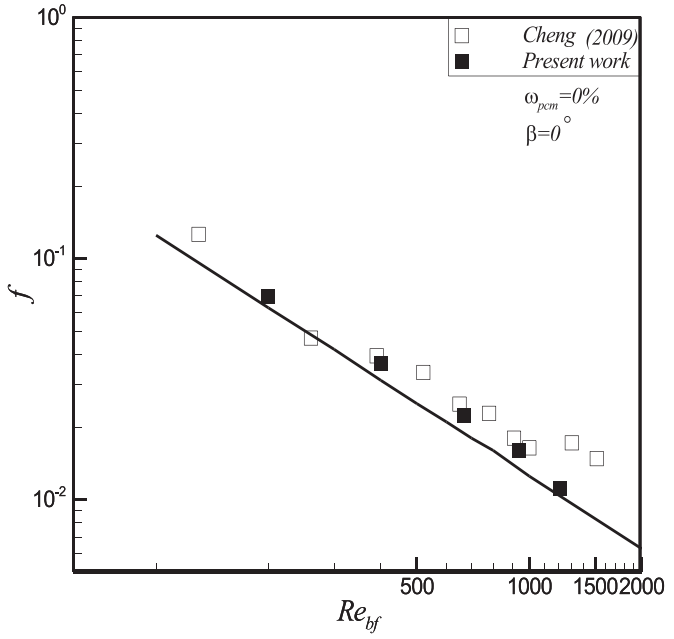

Fig. 6. Comparison of the friction factor f of the present study with the literature results.

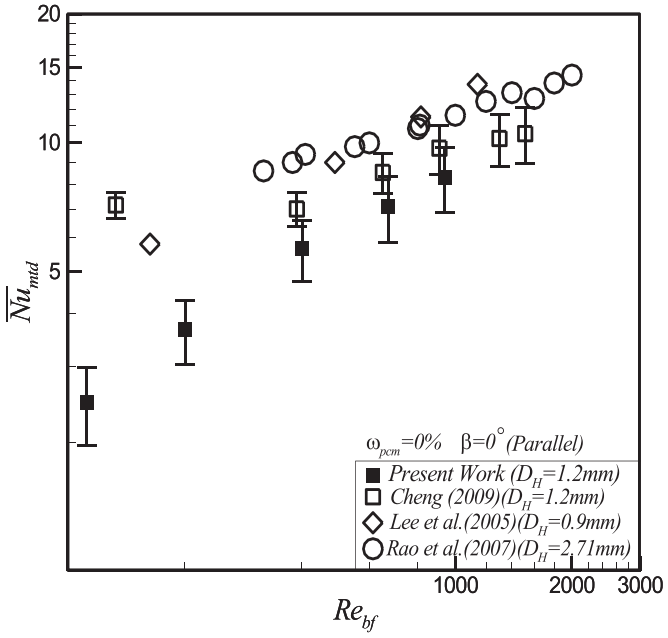

Fig. 7. A comparison of the average Nusselt number ($\overline{Nu}_{mtd}$) with the literature-works of Cheng [36], Lee et al. [39], and Rao et al. [20].

4.1. Validation

The results of the present experiment are compared with the available literature works for the case of pure water. The friction factor of the present study is compared with the formula reported by Kandlikar et al. [38] and plotted in Fig. 6. As seen, there is a good agreement between the results of the present experiment and literature data. Fig. 6 shows that the measured friction factor is slightly larger than the theoretical value. This is since the flow is not fully developed at the early inlet sections of the channel. Moreover, Cheng [36] experimentally found that there could be a large deviation between the theoretical and measured friction factor at high Reynolds numbers, e.g., Re_{bf} = 403 ~ 940. For low Reynolds numbers, the deviation will be smaller, but the measurement error due to the accuracy of the flow and pressure sensors is high.

In the term of average Nusselt number ($\overline{Nu}_{mtd}$), the results are compared with the experiments of Lee et al. [39] for a hydraulic diameter of D_H = 0.9 mm. Rao et al. [20] investigated the effect of heat transfer in a channel with D_H = 2.7 mm for various working-fluids. Besides, Cheng [36] also discussed the heat transfer benefits of different working-fluids in a channel with D_H = 1.2 mm. The results of the present study are reported for D_H = 1.2 and various values of Re_{bf} for the case of pure water. As seen in Fig. 7, the trend of the results is in agreement with the literature-works and shows that the Nusselt number grows by the increase of Reynolds number. However, there is a gap between the Nusselt numbers of different studies, and this gap is more evident at low Reynolds numbers. In the case of small Reynolds numbers, the errors are higher due to the error of flow meter and pressure sensors. Moreover, the reason for the difference in Nusselt numbers could be due to the difference in the aspect ratios of the studies, heating-powers, and the total channels of the heatsinks. As mentioned in Lee et al. [39], the aspect ratio does affect the magnitude of the Nusselt number, and it raises by the growth of the aspect ratio. In the research of Cheng [36], the aspect ratio was 1.5, while the aspect ratios of the microchannels in the studies of Lee et al. [39] and Rao et al. [20] were 5.44 and 2.1, respectively. Hence, as can be seen in Fig. 7, the Nusselt number for the study of Lee et al. [39] is the highest, and the study of Rao et al. [20] is after that. The Nusselt numbers of the present study and those of Cheng [36] are the lowest as they own the lowest aspect ratio of 1.5.

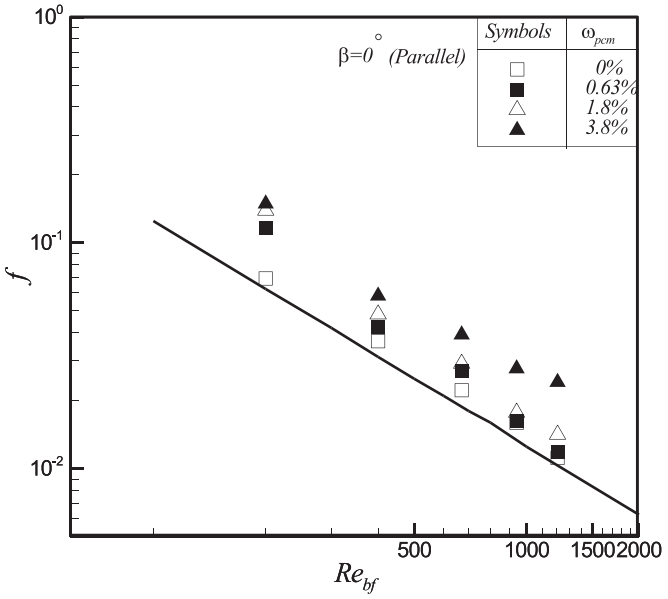

Fig. 8. Relation between friction factor and Reynolds number for various volume fractions of NEPCM particles.

Fig. 8 shows the effect of various volume fractions of NEPCM nanoparticles on the friction factor. As seen, the raise of the NEPCM volume fraction boost the friction factor. Attention to row data denotes that the increase of volume fraction of NEPCM particles raises the pressure drop across the microchannel, which is due to the increase in the viscosity of the suspension by the presence of NEPCM particles. The presence of 3.8% of NEPCM particles raises the viscosity of the suspension by 72%.

Figs. 9 and 10 depict the effect of using NEPCM-suspension on the non-dimensional wall temperature for various volume fractions of NEPCM particles. Figs. 9 and 10 are plotted for the main heating plate powers of 20 W and 30 W, respectively. The results show that

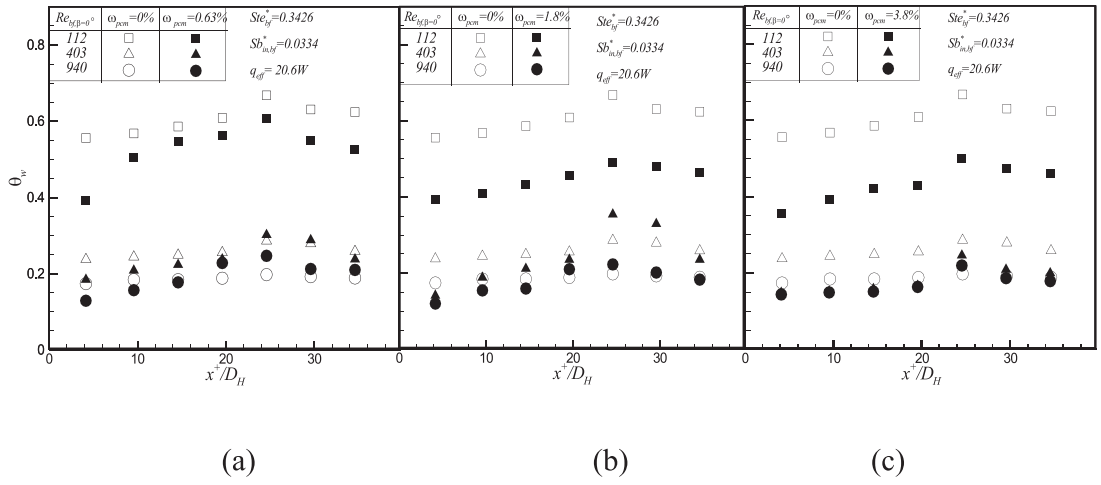

Fig. 9. Dimensionless wall temperature distribution for various volume fractions of NEPCM particles when the heating-power is 20 W. The comparison of the results with the pure water (ω_{pcm} = 0.0%) when (a) ω_{pcm} = 0.63%, (b) ω_{pcm} = 1.8%, and (c) ω_{pcm} = 3.8%.

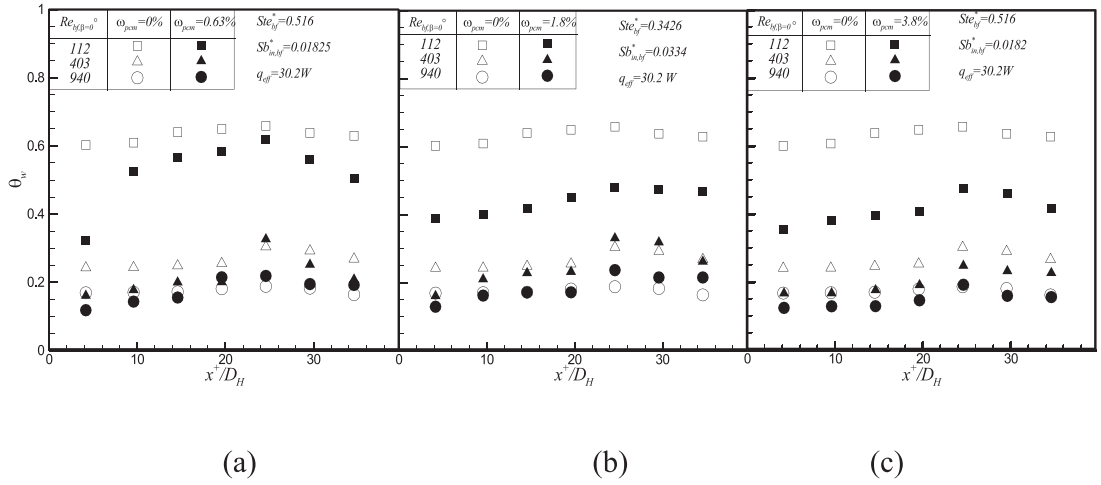

Fig. 10. Dimensionless wall temperature distribution for various volume fractions of NEPCM particles when the heating-power is 30 W. The comparison of the results with the pure water (ω_{pcm} = 0.0%) when (a) ω_{pcm} = 0.63%, (b) ω_{pcm} = 1.8%, and (c) ω_{pcm} = 3.8%.

the presence of NEPCM particles reduces the channel wall temperature regardless of the amount of heat flux when the Reynolds number is small. The raise of NEPCM volume fraction from 063% to 1.8% drops the overall wall temperature along the microchannel, which indicates the enhancement of the heat transfer. Interestingly, increasing the volume fractions of NEPCMs from 1.8% to 3.8% shows a minimal variation of wall temperature along the microchannel. Fig. 9 reveals that raising the Reynolds number to 403 drops the overall wall temperature, but the increase of Reynolds number reduces the significance of the presence of NEPCM particles regardless of the amount of NEPCM volume fraction. In the case of Re_{bf} = 403 and more obviously in the case of 940, the presence of NEPCM particles can raise the wall temperature at certain locations of the microchannel after the mid-length of the channel toward the outlet. The same trend of results can be observed for the higher heating-power of 30 W in Fig. 10. This figure also shows that the presence of NEPCM particles at the middle range of Reynolds number, e.g., Re_{bf} = 403, can be beneficial when the heat flux is high. In the cases of Re_{bf} = 403 and 0.63% of NEPCM particles, the wall temperature is almost similar to the pure water when the heating-power is 20. However, at the same Reynolds number and by increasing the heating-power to 30 W, the presence of NEPCM particles results in a drop of wall temperature.

From the trend of the results of Figs. 9 and 10, it can be concluded that the time scale of the fluid which passes through the channel is important. When the Reynolds number is small, the working-fluid moves slowly in the channel, and the NEPCM particles have enough time to absorb the heat and contribute to the heat transfer by their latent heat. However, when the Reynolds number increases, the working-fluid quickly leaves the microchannel. Therefore, at high Reynolds numbers, the heat transfer is dominated by sensible heat capacity. As seen in Table 2, the presence of NEPCM particles reduces the sensible heat capacity of the working-fluid, i.e., $\rho \times c_p$. Therefore, the presence of NEPCM particles could increase the local wall temperature when the Reynolds number is high.

Fig. 11 exhibits the average Nusselt number as a function of the Reynolds number (Re_{bf}) for various volume fractions of NEPCM particles in terms of $\omega_{pcm}/(Ste^* \times (1+Sb_{in}^*))$. Fig. 11(a), (b), and (c) correspond to the heating-powers of 10 W, 20 W, and 30 W, respectively. Here, the average Nusselt number can be considered as the characteristic parameter of the overall heat transfer. The increase of the Nusselt number indicates the improvement of heat transfer in the microchannel and, consequently, in the heatsink. Fig. 11(a) shows that the increase of the volume fraction of NEPCM particles elevates the average Nusselt number regardless of the amount of provided heating-power when the Reynolds number is small

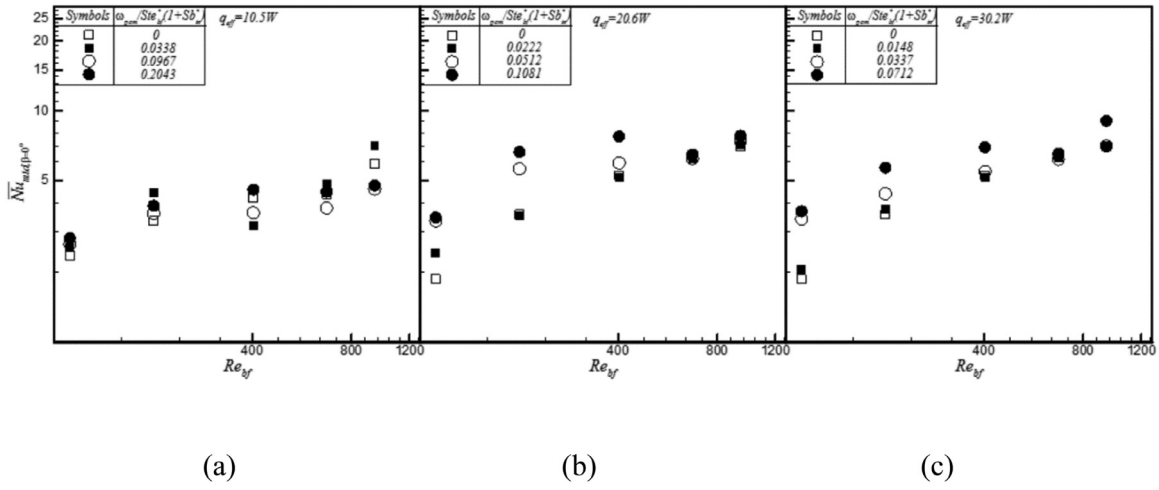

Fig. 11. The average Nusselt number ($\overline{Nu}_{mtd}$) as a function of Re_{bf} for various heat capacity ratios ($\omega_{pcm}/[Ste^* \times (1 + Sb_{in}{}^*)]$) when the heating-power is (a) 10 W%, (b) 20 W, and (c)30 W.

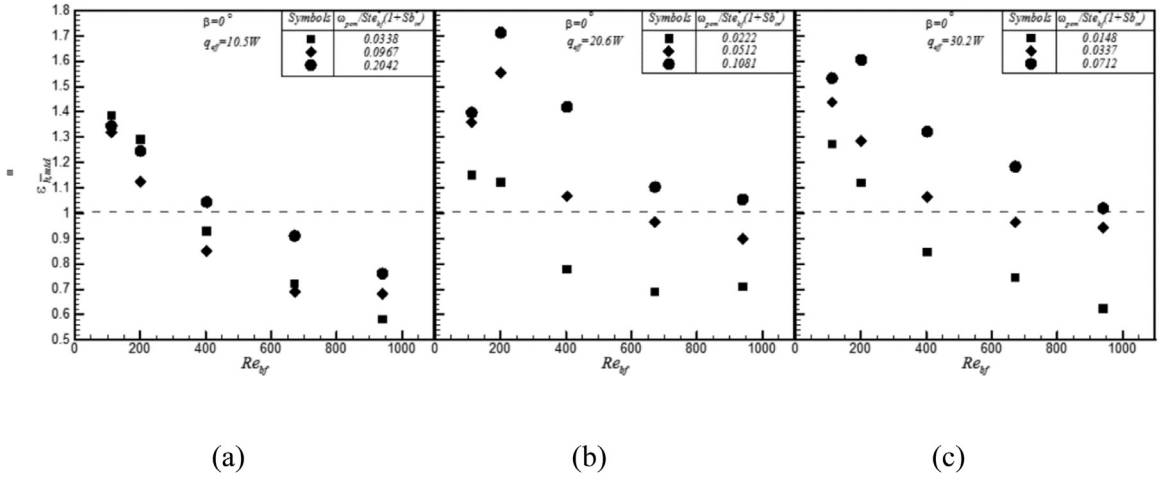

Fig. 12. The convection ($\varepsilon_{\overline{h}mtd}$) as a function of Re_{bf} for various heat capacity ratios ($\omega_{pcm}/[Ste^* \times (1 + Sb_{in}{}^*)]$) when the heating-power is (a) 10 W%, (b) 20 W, and (c) 30 W.

(Re_{bf} = 112~201). This trend of the results is in full agreement with the reduction of wall temperature by the presence of NEPCM particles at low Reynolds numbers, which was observed in Figs. 9 and 10.

The trend of the results shows that there is a turning point Reynolds number, in which the effect of the presence of NEPCM particles reversed. The turning point Reynolds number is a function of the heating-power, and it about Re_{bf} = 403 and Re_{bf} = 672, for the heating-powers of 20 W and 30 W, respectively. This turning point can be considered as a critical Reynolds number for the advantage or disadvantage of using NEPCMs. Here, the raise of the heating-power increases the critical Reynolds number. The same trend of behavior was also observed for the local profiles of non-dimensional wall temperature in Figs. 9 and 10. As mentioned, the time scale of latent heat transfer and the staying-time of the working-fluid in the microchannel are the influential parameters. For small time scales, the sensible heat capacity is the dominant heat transfer mechanism, while the contribution of the latent heat transfer is considerable for a larger time scale. The increase of the heating-power boosts the temperature difference between the working-fluid and the microchannel wall, and it intensifies the contribution of the latent heat mechanism. Hence, the variation of the heating-power shifts the critical Reynolds number.

Fig. 12 displays the convection ratio, $\varepsilon_{\overline{h}mtd}$, for various values of Reynolds number at three heating-powers of 10 W%, 20 W, and 30 W. As seen, the highest value of $\varepsilon_{\overline{h}mtd}$ occurs at Reynolds number of 201 and a heat capacity ratio of 0.1080 ($\omega_{pcm}/[Ste^* \times (1+Sb_{in}{}^*)]$=0.1080), which corresponds to the heating-power of 20 W. In Fig. 12, the maximum convection ratio shows a 70% improvement of heat transfer. Generally, the convection ratio ($\varepsilon_{\overline{h}mtd}$) is higher for low Reynolds flows and high values of the heat capacity ratio.

The results of this experiment show that a better convection ratio can be achieved if the staying-time of working-fluid in the microchannel (time scale of heat transfer) extends, and the heating-power increases. The extension of the staying-time improves the heat transfer by the contribution of the latent heat, while the rise of the heating-power increases the conduction heat transfer mechanism, which indirectly boosts the contribution of latent heat transfer. It should be noted that the convection ratio is bellow unit for high Reynolds numbers, which confirms the reduction of heat transfer in the microchannel by using NEPCMs.

Fig. 13 illustrates the performance index (FOM) as a function of Reynolds number for various values of the heat capacity ratio at different heating-powers. The FOM shows the ratio of the convection ratio to the amount of the consumed pumping power. Indeed, FOM compares the improved heat transfer coefficient to the increased pumping power to judge if the improvement of heat transfer is cost-efficient. The trend of the behavior of the FOM can be similar to the convection ratio, which was investigated in

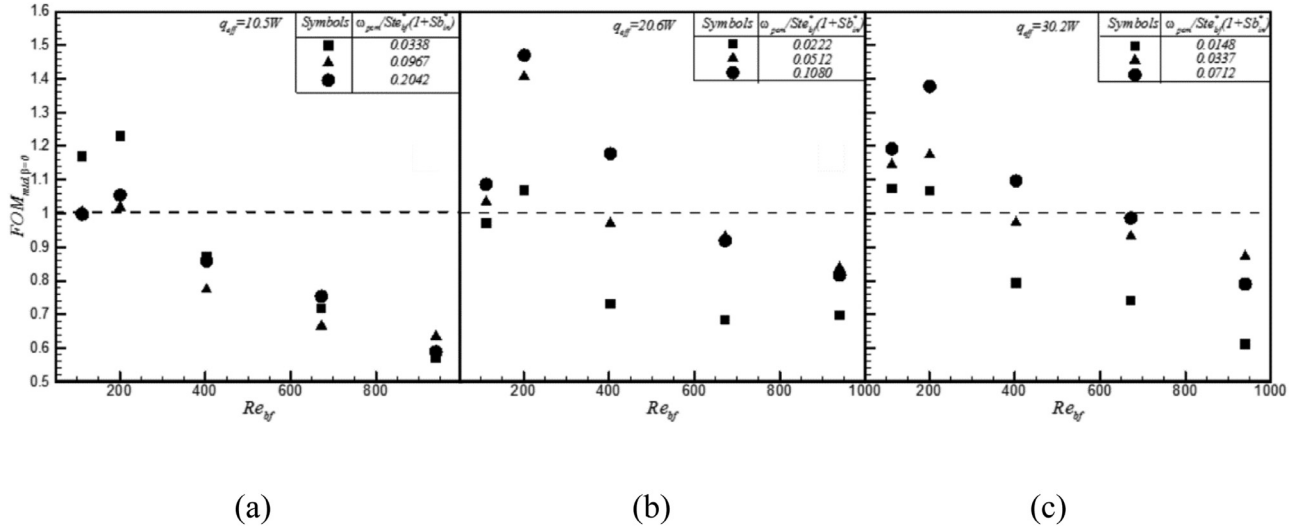

Fig. 13. The Performance index (FOM_{mtd}) as a function of Re_{bf} for various heat capacity ratios ($\omega_{pcm}/[Ste^* \times (1 + Sb_{in}{}^*)]$) when the heating-power s (a) 10 W%, (b) 20 W, and (c) 30 W.

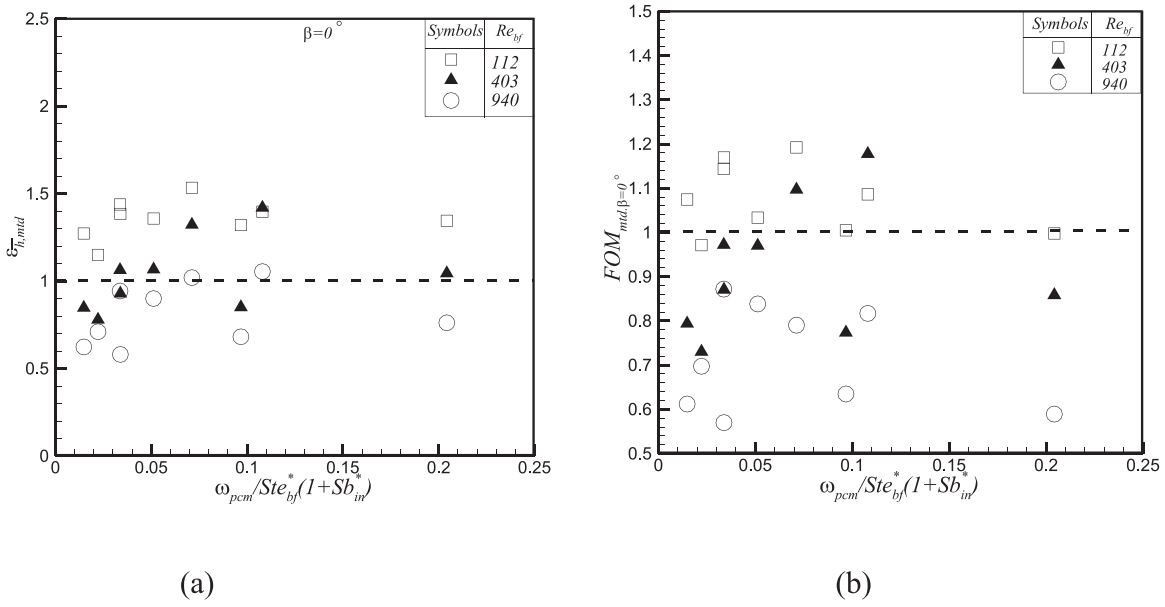

Fig. 14. The maps of heat transfer as a function of heat capacity ratio ($\omega_{pcm}/[Ste^* \times (1 + Sb_{in}{}^*)]$) for various values of Re_{bf} for (a) convection ratio ($\varepsilon_{\overline{h}mtd}$), and (b) performance index (FOM_{mtd}).

Fig. 12, while the consumed pumping power depends on the viscosity variation and may change the overall trend of the performance index (FOM). Fig. 13 depicts that the highest value of FOM, which is 1.45, corresponds to the case of maximum convection ratio ($\varepsilon_{\overline{h}mtd}$) at $Re_{bf} = 201$. Thus, heat transfer was the dominant effect on the cost-efficiency of heat transfer (FOM).

Figs. 14(a) and 14(b) show the map of convection ratio, and performance index, respectively. The maps are plotted for various heat capacity ratios ($\omega_{pcm}/[Ste^* \times (1 + Sb_{in}{}^*)]$) and Reynolds numbers. As seen, a convection ratio of 40% can be achieved by using NECPM at the Reynolds number of 112 and the heat capacity ratio of 0.108. Considering the heat transfer of micron-size capsules, Sabbah et al. [40]. theoretically investigated the flow and heat transfer of a slurry of MECPM in a microchannel heatsink and found that the maximum convection ratio can reach about 43% for the case of a minimum Reynolds number of 100 and the heat capacity ratio of 0.11. Fig. 14(a) indicates that the highest value of the convection ratio, which is 70%, appears at the Reynolds number 201 and the heat capacity ratio of 0.1080 by using nanocapsules. Fig. 14(b) shows that the performance index is high at low Reynolds numbers, where the convection ratio is significant. The performance index is lower than the unit at high Reynolds numbers, indicating the inefficiency of using NEPCMs at high flow rates. The reduction of performance index is due to the drop in the convection ratio and the growth of the required pumping power at high flow rates, which is due to the growth of the working-fluid viscosity by the presence of NEPCM particles.

Fig. 15 shows the COP as a function of Reynolds number for the pure water and various values of the volume fraction of NEPCM particles. This figure shows that COP has an inverse relation to the volume fraction of NEPCM particles. Indeed, COP compares the actual heat transfer to the required pumping power. Since the heat losses are quite small due to the well-insulation of the test module, the changes of the COP are related to the pumping powers. The increase of the volume fraction of NECPM particles raises the

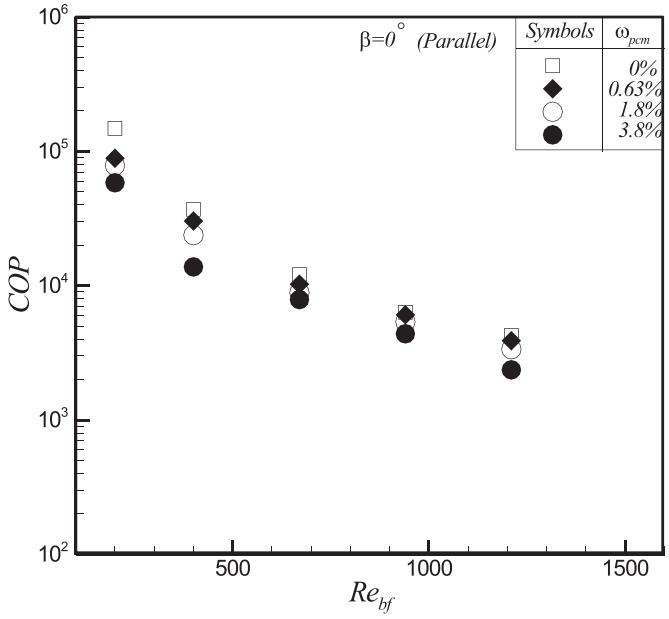

Fig. 15. Relation between COP and Reynolds number for various volume fractions of NEPCM particles.

required pumping power by boosting the viscosity of the working-fluid. Thus, the increase of ω_{pcm} results in a significant drop in COP.

5. Conclusion

In this study, the heat transfer performance of dispersing NEPCM particles in water was addressed in a microchannel of a heatsink. The NEPCM were synthesized using of eicosane as core and formaldehyde as the shell. The size of the achieved phase change nanoparticles was in the range of 250–350 nm. The impact of using various concentrations of NEPCM particles is examined on the microchannel wall temperature, Nusselt number, convection ratio, performance index (FOM), and COP. The main outcomes of the present experimental study can be summarized as follows:

1 Using NEPCM-water suspension reduces the wall temperature considerably when the Reynolds number is low. Hence, to fully utilize the latent heat value of the phase change material, it is necessary to reduce the flow rate, increase the concentration, and extend the time of passing NEPCM particles in the channel. When the Reynolds number is low, the presence of NECPM particles unconditionally enhances the heat transfer for all of the experiment parameters. However, when the Reynolds number is high, the deterioration of the heat transfer rate can be observed by the presence of NEPCM particles.
2 The increase of the heating-power improves the heat transfer rate and convection ratio of using NECPM-suspensions. A higher concentration of NEPCM particles is of interest to higher heating-powers.
3 The convection ratio is the best at low flow rates, and the increase in the flow rate reduces the advantages of using NEPCMs and the convection ratio. However, the maximum value of the convection ratio occurs at $Re_{bf} = 201$ instead of $Re_{bf} = 100$, which indicates the strong influence of thermophysical properties on the thermal behavior of NEPCM-suspension.
4 The performance index (FOM_{mtd}) is best at low flow rates. This is because the heat transfer rate is high, and the pump power is not too large at small Reynolds numbers. The maximum value of the performance index (FOM_{mtd}) occurred at $Re_{bf} = 201$, which corresponds to the highest heat transfer enhancement (convection ratio). At this low flow rate, the increase of the pumping power is small, and hence, it does not change the trend of the behavior of the performance index. However, at high flow rates, i.e., high Reynolds numbers, the performance index drops notably as the convection ratio drops, and the pumping power raises due to the increase of viscosity.

The results of the present study show that the NEPCMs are practical for low Reynolds numbers; however, the measurement range limit of the utilized differential pressure-sensor does not allow testing Reynolds numbers below 100 in the current microchannel. Using a more sensitive pressure sensor, covering a lower range of flow rates and pressure drops, is required to explore lower flow rates, which can be subject to future studies.

Moreover, by attention to the trend of thermal behavior of the NEPCM-suspension, it was concluded that the suspension does not stay enough in the channel to reach its latent heat capacity potential fully. Hence, one way of extending the staying-time of the suspension in the microchannel was reducing the flow rate. Another way is changing the geometrical design of the microchannel heatsink to extend the staying-time of the suspension inside the heatsink, which can be subject to future investigations.

Declaration of Competing Interest

The authors clarify that there is no conflict of interest for report.

CRediT authorship contribution statement

C.J. Ho: Conceptualization, Methodology, Supervision, Writing - original draft, Writing - review & editing. **Yen-Chung Liu:** Conceptualization, Methodology, Validation, Formal analysis, Data curation. **Mohammad Ghalambaz:** Investigation, Writing - review & editing, Validation, Formal analysis. **Wei-Mon Yan:** Investigation, Validation, Formal analysis, Writing - review & editing.

Acknowledgements

The authors appreciate the financial support from Ministry of Science and Technology, Taiwan, under grant number MOST 106-2221-E-027-103. The authors also acknowledge the financially supported by the “Research Center of Energy Conservation for New Generation of Residential, Commercial, and Industrial Sectors” from The Featured Areas Research Center Program within the framework of the Higher Education Sprout Project by the Ministry of Education (MOE) in Taiwan.

References

[1] H.M. Ali, Applications of combined/hybrid use of heat pipe and phase change materials in energy storage and cooling systems: a recent review, J. Energy Storage 26 (2019) 100986.
[2] H.M. Ali, Recent advancements in PV cooling and efficiency enhancement integrating phase change materials based systems–A comprehensive review, Sol. Energy 197 (2020) 163–198.
[3] A. Hassan, A. Wahab, M.A. Qasim, M.M. Janjua, M.A. Ali, H.M. Ali, T.R. Jadoon, E. Ali, A. Raza, N. Javaid, Thermal management and uniform temperature regulation of photovoltaic modules using hybrid phase change materials-nanofluids system, Renew. Energy 145 (2020) 282–293.
[4] H.M. Ali, Experimental study on the thermal behavior of RT-35HC paraffin within copper and Iron-Nickel open cell foams: energy storage for thermal management of electronics, Int. J. Heat Mass Transf. 146 (2020) 118852.
[5] D.B. Tuckerman, R.F.W. Pease, High-performance heat sinking for VLSI, IEEE Electron Dev. Lett. 2 (5) (1981) 126–129.
[6] F.T. Kanizawa, C.B. Tibiriçá, G. Ribatski, Heat transfer during convective boiling inside microchannels, Int. J. Heat Mass Transf. 93 (2016) 566–583.
[7] A.J. Chamkha, M. Molana, A. Rahnama, F. Ghadami, On the nanofluids applications in microchannels: a comprehensive review, Powder Technol. 332 (2018) 287–322.

[8] L. Snoussi, N. Ouerfelli, K. Sharma, N. Vrinceanu, A. Chamkha, A. Guizani, Numerical simulation of nanofluids for improved cooling efficiency in a 3D copper microchannel heat sink (MCHS), Phys. Chem. Liq. 56 (3) (2018) 311–331.
[9] B. Gireesha, B. Mahanthesh, A.J. Chamkha, Entropy generation analysis of magneto-nanoliquids embedded with aluminium and titanium alloy nanoparticles in microchannel with partial slips and convective conditions, Int. J. Numer. Methods Heat Fluid Flow (2018).
[10] C.J. Ho, L.C. Wei, Z.W. Li, An experimental investigation of forced convective cooling performance of a microchannel heat sink with Al2O3/water nanofluid, Appl. Therm. Eng. 30 (2–3) (2010) 96–103.
[11] K. Saito, M.F. Taras, Multipass microchannel heat exchanger, Google Pat. (2019).
[12] R.T. Miller, S. Schon, Laminated microchannel heat exchangers, Google Pat. (2019).
[13] T. Vu, T.N. Tran, J. Xu, Single-phase flow and heat transfer characteristics of ethanol/polyalphaolefin nanoemulsion fluids in circular minichannels, Int. J. Heat Mass Transf. 113 (2017) 324–331.
[14] V. Trinh, J. Xu, An experimental study on flow and heat transfer characteristics of ethanol/polyalphaolefin nanoemulsion flowing through circular minichannels, Nanoscale Res. Lett. 12 (1) (2017) 216.
[15] F. Zewede, H. Argaw, T. Tran, J. Xu, Convective Heat Transfer of Ethanol/Polyalphaolefin Nanoemulsion Inside Circular Minichannel Heat Exchanger, ASME 2017 Heat Transfer Summer Conference, American Society of Mechanical Engineers Digital Collection, 2017.
[16] C.J. Ho, C.S. Huang, C. Qin, W.M. Yan, Thermal performance of phase change nano-emulsion in a rectangular minichannel with wall conduction effect, Int. Comm. Heat Mass Transf. 110 (2020) 104438.
[17] M.M. Farid, S. Al-Hallaj, Microchannel heat exchanger with micro-encapsulated phase change material for high flux cooling, Google Pat. (2012).
[18] R. Shaukat, M.S. Kamran, S. Imran, Z. Anwar, H. Ali, Numerical investigation of melting heat transfer during microencapsulated phase change slurry flow in microchannels, J. Enhanc. Heat Transf. 26 (6) (2019).
[19] N.S. Roberts, R. Al-Shannaq, J. Kurdi, S.A. Al-Muhtaseb, M.M. Farid, Efficacy of using slurry of metal-coated microencapsulated PCM for cooling in a micro-channel heat exchanger, Appl. Therm. Eng. 122 (2017) 11–18.
[20] Y. Rao, F. Dammel, P. Stephan, G. Lin, Convective heat transfer characteristics of microencapsulated phase change material suspensions in minichannels, Heat Mass Transf. 44 (2) (2007) 175–186.
[21] L. Chow, J.-H. Du, A. Gupta, K. Kota, R. Kumar, S. Kuravi, Microchannel heat sink with micro encapsulated phase change material (MEPCM) slurry, Univ. Cent. Fl. Orlando Office Res. Commer. (2009).
[22] W. Wu, H. Bostanci, L. Chow, Y. Hong, C. Wang, M. Su, J.P. Kizito, Heat transfer enhancement of PAO in microchannel heat exchanger using nano-encapsulated phase change indium particles, Int. J. Heat Mass Transf. 58 (1–2) (2013) 348–355.
[23] C.J. Ho, W.C. Chen, W.M. Yan, M. Amani, Cooling performance of MEPCM suspensions for heat dissipation intensification in a minichannel heat sink, Int. J. Heat Mass Transf. 115 (2017) 43–49.
[24] M.I. Hasan, H.L. Tbena, Numerical investigation of microchannel heat sink with MEPCM suspension with different types of PCM, Al-Qadisiyah J. Eng. Sci. 11 (1) (2018) 115–133.
[25] C.J. Ho, P.C. Chang, W.M. Yan, P. Amani, Efficacy of divergent minichannels on cooling performance of heat sinks with water-based MEPCM suspensions, Int. J. Therm. Sci. 130 (2018) 333–346.
[26] A. Sarı, C. Alkan, C. Bilgin, A. Bicer, Preparation, characterization and thermal energy storage properties of micro/nano encapsulated phase change material with acrylic-based polymer, Polymer Science, Ser. B 60 (1) (2018) 58–68.
[27] E. Alehosseini, S.M. Jafari, Micro/nano-encapsulated phase change materials (PCMs) as emerging materials for the food industry, Trends Food Sci. Technol. (2019).
[28] J.M. Khodadadi, Nanoparticle-enhanced phase change materials (NEPCM) with improved thermal energy storage, Google Pat. (2015).
[29] C. Zhang, T. Wang, D. Chen, F. Hong, P. Cheng, Confined jet array impingement cooling with spent flow distraction using NEPCM slurry, Int. Commun. Heat Mass Transf. 77 (2016) 140–147.
[30] H.R. Seyf, Z. Zhou, H. Ma, Y. Zhang, Three dimensional numerical study of heat-transfer enhancement by nano-encapsulated phase change material slurry in microtube heat sinks with tangential impingement, Int. J. Heat Mass Transf. 56 (1–2) (2013) 561–573.
[31] A. Petrovic, D. Lelea, I. Laza, The comparative analysis on using the NEPCM materials and nanofluids for microchannel cooling solutions, Int. Commun. Heat Mass Transf. 79 (2016) 39–45.
[32] M. Ghalambaz, S. Mehryan, A. Hajjar, A. Veisimoradi, Unsteady natural convection flow of a suspension comprising nano-encapsulated phase change materials (NEPCMs) in a porous medium, Adv. Powder Technol. (2019).
[33] A. Hajjar, S. Mehryan, M. Ghalambaz, Time periodic natural convection heat transfer in a nano-encapsulated phase-change suspension, Int. J. Mech. Sci. 166 (2020) 105243.
[34] M. Ghalambaz, A.J. Chamkha, D. Wen, Natural convective flow and heat transfer of Nano-Encapsulated Phase Change Materials (NEPCMs) in a cavity, Int. J. Heat Mass Transf. 138 (2019) 738–749.
[35] M. Ghalambaz, T. Groşan, I. Pop, Mixed convection boundary layer flow and heat transfer over a vertical plate embedded in a porous medium filled with a suspension of nano-encapsulated phase change materials, J. Mol. Liq. 293 (2019) 111432.
[36] W.C. Cheng, Heat Transfer Experiment On Forced Convection Performance of Water-Based Suspensions of Nanoparticles And/Or MEPCM Particles in a Minichannel Heatsink, National Cheng Kung University, Taiwan, 2009 Master thesis.
[37] J.F. Su, X.Y. Wang, H. Dong, Micromechanical properties of melamine–formaldehyde microcapsules by nanoindentation: effect of size and shell thickness, Mater. Lett. 89 (2012) 1–4.
[38] S.G. Kandlikar, S. Garimella, D. Li, S. Colin, M.R. King, Heat Transfer and Fluid Flow in Minichannels and Microchannels, Elsevier Ltd, Oxford, UK, 2006.
[39] P.-S. Lee, S.V. Garimella, D. Liu, Investigation of heat transfer in rectangular microchannels, Int. J. Heat Mass Transf. 48 (9) (2005) 1688–1704.
[40] R. Sabbah, M.M. Farid, S. Al-Hallaj, Micro-channel heat sink with slurry of water with micro-encapsulated phase change material: 3D-numerical study, Appl. Therm. Eng. 29 (2–3) (2009) 445–454.